The role of spatial shifting in El Niño/Southern Oscillation complexity

Sulian Thual, Boris Dewitte

The role of spatial shifting in El Niño/Southern Oscillation complexity

Sulian Thual[1*] and Boris Dewitte[1,2,3]

[1*]CECI, CERFACS/CNRS, 42 Avenue G. Coriolis, Toulouse, 31057, France.
[2]Department, CEAZA, Raúl Bitrán 1305, La Serena, 1700000, Chile.
[3]Departamento de Biología Marina, Facultad de Ciencias del Mar, Universidad Católica del Norte, Larrondo 1281, Coquimbo, 1780000, Chile.

*Corresponding author(s). E-mail(s): sthual@cerfacs.fr;

Abstract

The El Niño-Southern Oscillation (ENSO) represents the most consequential fluctuation of the global climate system, with dramatic societal and environmental impacts.[1,2] Its general dynamics are reasonably well understood and they involve ocean-atmosphere interactions that modify the Walker circulation in the equatorial Pacific.[3,4] However, some of its space-time features remain stubbornly elusive such as its event-to-event diversity and asymmetry.[5,6] Here we show that the spatial shifting movements of the Walker circulation control the ENSO space-time complexity[7] in a major way. We encapsulate these movements in a minimal model by simply reframing the general geometry of conventional recharge-discharge linear dynamics.[8] With this modification alone, the model captures altogether the essential ingredients of ENSO diversity, asymmetry, nonlinearity, non-normality and leading principal components.[5,6,9] It also manages to do so in substantially simpler fashion than previously considered, which improves our ability to address ENSO complexity.[7] The present paradigm of spatial shifting participates towards a more unified understanding of the ENSO, with potentially far reaching implications down the lines of modelling and prediction.

Keywords: El-Niño Southern Oscillation, Walker Circulation, Conceptual Models

1 Introduction

The El Niño-Southern Oscillation (ENSO), which refers collectively to the alternation between El Niño and La Niña events in the equatorial Pacific, affects extreme weather, populations and ecosystems worldwide.[1,2] Its impacts are however highly variable and unpredictable due to a considerable diversity in characteristics from one event to the next. Although most El Niño events are characterized by modest sea surface temperature (SST) warming in the central Pacific, a few of them stand out by a strong SST warming in the eastern Pacific with much more severe impacts.[10,11] For instance, the record eastern Pacific El Niño of 1997-98 induced catastrophic floods along the western coasts of both North and South America, droughts over the maritime continent in Southeast Asia as well as an increased tropical cyclone activity over the Pacific.[12] La Niña events, characterized by moderate cooling in the central to eastern Pacific, tend to yield similar although spatially displaced climate impacts.[1] Beyond disrupting the global atmospheric and oceanic structures, major ENSO events can be highly detrimental to both populations and ecosystems in terms of fisheries, tropical diseases spread, coral reef bleaching, and so on.[2] Understanding and predicting the ENSO's event-to-event diversity is thus a fundamental yet unreached goal in climate sciences.[13]

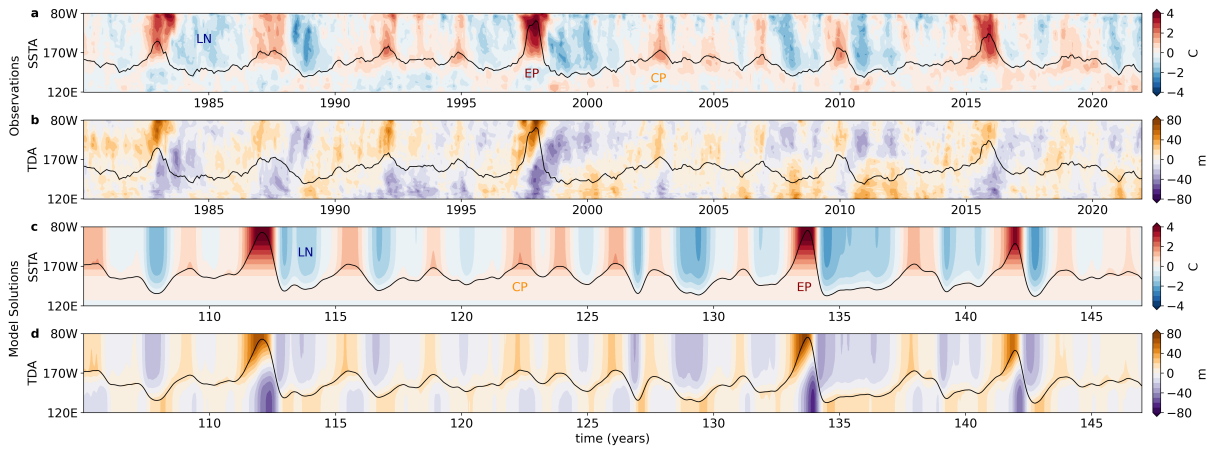

Fig. 1 Observed and modelled ENSO variability. **a,b**, Time-longitude hovmollers of sea surface temperatures anomalies (SSTA) and thermocline depth anomalies (TDA) in the equatorial Pacific, as computed from observations (averaged 5°N-5°S with seasonal variations removed). Solid lines in each panel indicate the longitudinal position of the warm pool edge (i.e. 29°C SST isotherm, see methods). **c,d**, Hovmollers repeated for solutions generated by a minimal oscillator model, displayed over a hand-picked period with time relative to the beginning of numerical simulation. The model reasonably reproduces all major ENSO patterns: El Niños with strong eastern Pacific warming (EP), with moderate central to eastern Pacific warming (CP), and La Niñas with moderate and lingering cooling that extends further westward (LN).

Despite the primary importance of the ENSO and the decades of research progress, present-day general circulation models with full-physics still tend to represent it with some bias as regards it amplitude, spatial pattern or evolution, among others.[14,15] Similar issues arise in models of decreased complexity that, despite reasonably depicting the ENSO in terms of coupled interactions between the atmosphere and ocean, differ in terms of the processes invoked for its more advanced features.[4,9,16] A major reason for these shortcomings is, generally speaking, a lack of consensus for understanding the ENSO's nonlinear dynamics. For example, even though El Niño events are commonly classified into the central Pacific or eastern Pacific type, which is referred to as ENSO diversity, it is still debated whether these stem from a continuum or from separate modes of variability.[5,17,18] Another lack of consensus regards the processes by which El Niño events may reach larger amplitudes yet shorter durations than La Niña events, which is referred to as ENSO asymmetry or non-normality.[6,19,20] Although significant progress has been made, there is no generally accepted theory that provides a complete and comprehensive picture of the ENSO space-time complexity.[7]

Here we propose a model that captures the essential ingredients of ENSO complexity discussed above such as its diversity and asymmetry in spatial patterns and evolution (Fig. 1). The present model manages to do so in extremely simple fashion: it is a minimal oscillator with only two core variables and one source of randomized forcing, that extends commonly accepted recharge-discharge theory[8] but does not introduce any sophisticated mechanism. Its novelty consists in reframing the main geometry of the ENSO, which simplifies the problem but also questions the ENSO's generally accepted degree of complexity. Hereafter we detail the model's rationale and properties as well as the broader implications for predicting ENSO variability and impacts.

2 Model Geometry

The formulation of the present oscillator model starts by proposing an idealized geometry for the general circulation of the equatorial Pacific, commonly referred to as the Walker circulation (Fig. 2a).[3,21,22] We consider a longitudinal strip at the equator that represents the circulation in terms of two regions with distinct properties, the so-called warm pool and cold tongue regions. For simplicity, our representation is limited to zonal wind stress and SST at the ocean's surface as well as thermocline depth that roughly measures the

amount of heat stored below the surface. Such a representation is compelling here in that it is amenable to detailed analysis yet compares reasonably well with observations (Extended Data Fig. 1).

The Walker circulation is not static and its evolution is in fact what constitutes ENSO variability (Fig. 2b, c). The novelty of the present approach consists in representing such an evolution in rather simple terms, by directly shifting the entire Walker circulation back and forth in the longitudinal (i.e. zonal) direction. This generates La Niña events when the circulation shifts westward which expands the cold tongue region, and conversely El Niño events when the circulation shifts eastward which expands the warm pool region. Such a behavior is observed in nature in the form of general and coherent movements that follow the warm pool edge and that involve both the atmosphere and ocean (Extended Data Fig. 2, Supplementary Information Video 1).

Generally speaking, the Walker circulation can be decomposed into a mean state, representative of average (or seasonal) conditions, and anomalies, representative of departures i.e. of ENSO variability (Fig. 1). Conventional ENSO models typically simplify the problem by prescribing the mean state to focus on the ENSO anomalies.[4] This however, adds an unexpected layer of complexity as it accounts rather indirectly for the spatial movements of the total circulation.[23] In order to circumvent this difficulty, our representation focuses explicitly on the total circulation (minus seasonal effects) from which the mean state and anomalies are deduced but not prescribed.

3 Model Dynamics

Although fundamental, the process of Walker circulation shifting discussed above hasn't yet found a firm standing in ENSO theory with the exception of a few attempts at modelling the warm pool's edge position.[24,25] Here we encapsulate the process in a minimal oscillator with concise ENSO dynamics, which is achieved by extending a well proven and widely-used[9] theoretical framework, the so-called recharge-discharge oscillator.[8] As detailed in the methods section, a general form

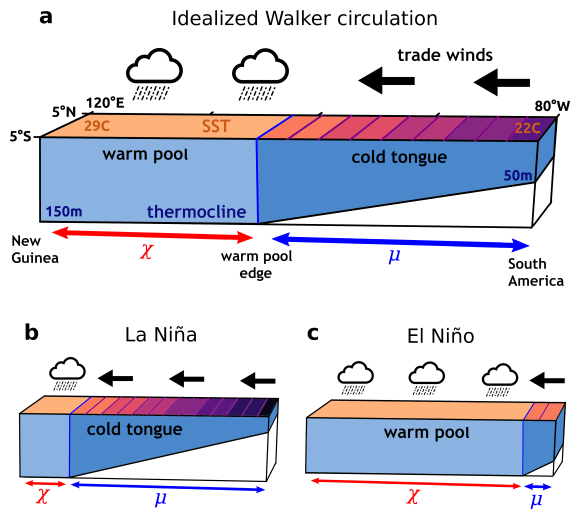

Fig. 2 Idealized Walker circulation. **a**, The equatorial Pacific is represented by a longitudinal strip divided into a warm pool region and a cold tongue region. The warm pool is characterized by saturating sea surface temperatures (SST), a deep thermocline and increased convection. The cold tongue is characterized by trade winds blowing west that gradually shallow the thermocline and cool the SST. **b,c**, The present approach consists in shifting the circulation as a whole during La Niña and El Niño while conserving its general geometrical features. This results in opposite contractions and expansions of each region as described by the variable extents χ and μ.

of the resulting system can be expressed as:

$$\begin{aligned} d\mu/dt &= -a_1\mu - b_1 h_M + c_1 - d_1\mu^2 \\ dh_M/dt &= -a_2 h_M + b_2\mu + c_2 + \zeta \end{aligned} \qquad (1)$$

where t is time, μ is the extent of the cold tongue region, h_M is basin-wide heat content,[8,26] ζ is a stochastic (i.e. randomized) forcing,[27] and the remainder consists of constant parameters. The above system generates ENSO-like oscillations that are irregular due to the stochastic forcing and that occasionally exhibit strong El Niño events as in nature (Fig. 3a, b).

The main novelty compared to conventional recharge-discharge theory is that, instead of fixing the domain of the cold tongue, we allow it to expand and contract by solving for its extent μ (Fig. 2). This allows capturing all major ENSO patterns as a single continuum:[5] La Niña (μ large), central Pacific El Niño (μ moderately small) and eastern Pacific El Niño (μ very small) (Fig. 1, 2). Such a modification nevertheless conserves the

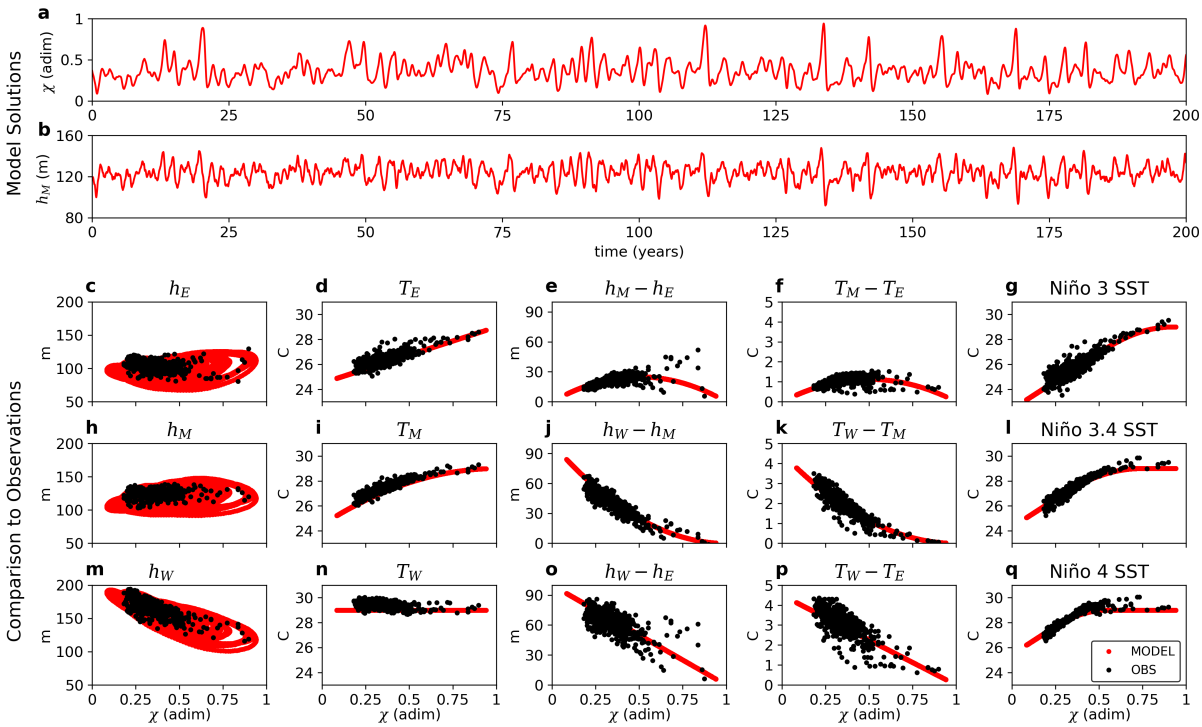

Fig. 3 Evolution of spatial averages. **a,b**, Timeseries of warm pool extent χ and basin-wide heat content h_M obtained from a numerical integration of the oscillator model (Eq. 1), and which represents ENSO variability. χ within 0-1 corresponds to a warm pool edge within 120°E-80°W (Fig. 1, 2). **c-q**, Scatterplots between spatial averages (or combinations of them) and warm pool extent χ as measured in either model outputs (red) or observations (black). The indices T_W, T_E, T_M (h_W, h_E, h_M) averages SST (thermocline depth) conditions respectively over the warm pool, cold tongue and entire basin (120°E-80°W). The conventional indices Niño 4, 3.4 and 3 SST average conditions over the central (160°E-150°W), central-eastern (170°W-120°W) and eastern (150°W-90°W) Pacific. All averages are within the equatorial band (5°N-5°S). The ENSO-like oscillations from panels a,b are encapsulated in panel h. The model solutions reasonably match observations for relationships that are either linear (d,n,o,p), nonlinear quadratic (e,f,i,j,k), nonlinear saturating (g,l,q) or nonlinear oscillatory (c,h,m). The Niño SST indices (g,l,q) saturate at around 29°C when the warm pool region overlaps their domain entirely.

original recharge-discharge mechanism responsible for the ENSO's reversal of conditions, that is: the more expanded the cold tongue, the more the trade winds recharge heat content (term $b_2\mu$) which in turns warms the surface and rebalances the Walker circulation (term $-b_1 h_M$), and conversely (Extended Data Fig. 3).

Another novel addition is a quadratic nonlinearity (term $-d_1\mu^2$) that stems directly from the Walker circulation's geometry as detailed hereafter. Such a nonlinearity here shapes the dynamics such as to generate an asymmetry in amplitude and duration between El Niño and La Niña, as in nature[6] (Extended Data Fig. 4). Meanwhile, the remainder of the system is more conventional: ζ in particular is an ad-hoc stochastic forcing that mimics the effect of random fluctuations in nature (e.g. wind bursts[28,27]) and excites the otherwise dissipated system.

4 Model Nonlinearities

Our representation of the Walker circulation's spatial shifting movements offers new perspectives for interpreting the multi-faceted aspects of ENSO nonlinearity and non-normality.[6] We provide an overview of this interplay in the form of spatial averages over various regions of the equatorial Pacific including the warm pool and cold tongue regions of variable extents (Extended Data Fig. 5). The relationships between these spatial averages and spatial shifting are nonlinear for the most part as per the model's formulation (see methods), yet all of them hold reasonably well in observations (Fig. 3c-q).

Importantly, the present model nonlinearities all stem from the general geometry of the problem rather than details of local processes (e.g. starting budgets), which differs from other rationales proposed in the literature.[19,20,27] For example, the thermocline's response to spatial shifting is geometrically quadratic (Fig. 3e, j), which in turn generates ENSO asymmetry as it mitigates La Niña development but amplifies El Niño development (Extended Data Fig. 6). As another example, the central to eastern Pacific is overlapped back and forth by either the warm pool or cold tongue which mixes nonlinearly saturating and sloping SST characteristics (Fig. 3g, l, q). This, in turn, provides a simple source of non-normality (e.g. skewness) for the resulting statistics[27,29] (Extended Data Tab. 1).

5 Principal Component Analysis

The first principal components (PCs) of SST in the equatorial Pacific deduce the leading ENSO patterns in terms of data covariance (see methods), but their interpretation still lacks consensus.[30,31] Here we reproduce the PC's overall characteristics for the first time with a minimal model (Fig. 4): this is not only achieved in terms of spatial structures but also in terms of a nonlinear quadratic relationship between PCs.[32,33]

The Walker circulation's longitudinal movements can in fact explain the PC's characteristics in reasonably simple terms. The first PC captures the cold tongue's movements over the eastern Pacific and approximately no variability from the warm pool's saturating SSTs over the western Pacific (Fig. 4a). The second PC captures a central Pacific variability (Fig. 4b) that stems from a spatial shifting nonlinearity mentionned earlier. As the central Pacific is overlapped back and forth by either the warm pool or cold tongue, it mixes saturating and sloping SST characteristics (Fig. 3q). The resulting characteristics have approximately a quadratic shape that is necessarily captured by a joint contribution of the first and second PCs, thus tying those together nonlinearly (Fig. 4c, Extended Data Fig. 7). Although our results suggest that the first PCs predominantly capture spatial shifting, they do not exclude the potential imprint of other phenomena from the literature.[34,35]

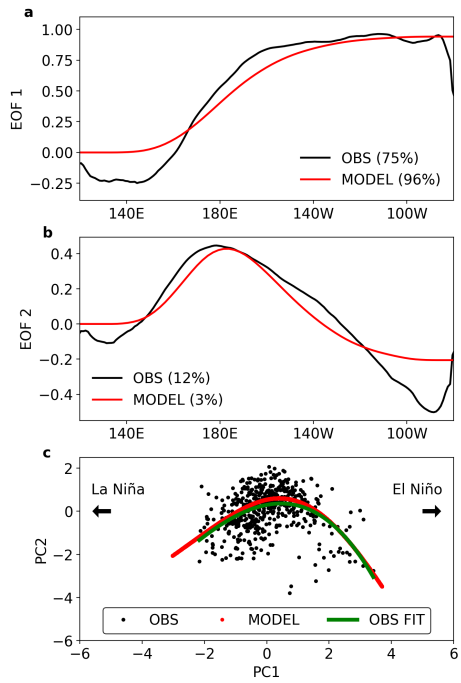

Fig. 4 Principal component analysis of SST. **a,b**, First and second Empirical Orthogonal Functions (EOFs) as computed from either model outputs (red) or observations (black), with explained variance indicated (%). **c**, Scatterplot between first and second principal component (PC) timeseries as computed from model outputs (red) or observations (black). The model solutions compare reasonably well with observations in terms of EOFs, explained variance and a quadratic relationship between PC timeseries (as highlighted in observations by a second order polynomial fit, green line). The first PC timeserie strongly correlates with spatial shifting (χ) in both the model (r=0.99) and observations (r=0.91). SST represent 5°N-5°S averages in the equatorial Pacific.

6 Outlook

Here we have shown that the spatial shifting movements of the Walker circulation shape the ENSO variability in a major way.[3] This allows reinterpreting some of the phenomenon's most complex and elusive features[7,5] using simple geometrical principles, as encapsulated in a minimal oscillator model. Our discovery suggests that the ENSO's nonlinear dynamics are simpler than previously considered to some extent, thus hopefully more predictable.[13]

Beyond improving ENSO understanding, the seminal concepts proposed here may shed a new light on other major aspects of the phenomenon. First and foremost, the present spatial shifting paradigm should be combined and reconciled with other rationales for complexity, nonlinearity and mean state interactions proposed in the literature, including in more realistic setups.[9,6,36] Far reaching implications extend to the study of teleconnections considering that the Walker circulation's movements are tied to pan-tropical as well as extra-tropical variability.[37,38] In fact, these interactions bridge not only ENSO-induced climate disruptions across the planet, but also remote influences on El Niño or La Niña onset.[1,2,39] Conjointly, our representation provides novel geometrical guidelines for the diagnosis of general circulation models, e.g. to infer core convective or dynamical feedbacks.[15,40,41] This, in turn, may help further understand how El Niño's strength and flavor are modulated by decadal variability and climate change.[33,42,43]

Acknowledgments. The research of S.T. is supported by ANR (Grant ANR-18-CE01-0012). B.D. acknowledges support from ANID (Concurso de Fortalecimiento al Desarrollo Científico de Centros Regionales 2020-R20F0008-CEAZA, Eclipse FSEQ210017 and COPAS COASTAL FB210021) and ANR (Grant ANR-18-CE01-0012). The authors thank O.Thual for discussions.

Competing interests. The authors declare no conflict of interest.

Authors' contributions. S.T. designed and performed research. S.T. and B.D. discussed research and wrote the paper.

Methods

Idealized Walker Circulation. Consider non-dimensional fields of SST T, thermocline depth h and zonal wind stress τ_x in a zonal strip representative of the equatorial Pacific (120°E to 80°W, averages 5°N to 5°S). Let the fields describe the evolution of an idealized Walker circulation (Fig. 2, Extended Data Fig. 1) that reads:

$$\begin{aligned}
&\text{if } x < \chi(t) \begin{cases} \tau_x(x,t) = 0 \\ T(x,t) = T_W \\ h(x,t) = h_W(t) \end{cases} \\
&\text{if } x \geq \chi(t) \begin{cases} \tau_x(x,t) = \tau_E \\ T(x,t) = T_W - 2s(x-\chi) \\ h(x,t) = h_W(t) - 2a(x-\chi) \end{cases}
\end{aligned} \tag{2}$$

where x is zonal position (with $0 \leq x \leq 1$) and t is time. The circulation is centered on the warm pool edge of position χ (pronounced "ki") that separates the warm pool region ($x < \chi$) from the cold tongue region ($x \geq \chi$) with distinct properties.

The structure of such a circulation results from a complex balance between the atmosphere and ocean in nature that is summarized here in its essential terms.[3,21,22,4] Trade winds (oriented westward) span the cold tongue region with constant intensity $\tau_E < 0$ where they induce SST as well as thermocline depth to slope at rates $2s$ and $2a$, respectively. Meanwhile, SSTs saturate at $T_W = 29°\text{C}$ over the warm pool region. In fact, SSTs nearing that threshold significantly increase convective activity in the atmosphere, which in turn captures excess heating. Convective activity reinforces the trade winds over the cold tongue through large scale convergence but also approximately breaks them down over the warm pool through the buildup of smaller scales fluctuations (e.g. wind bursts[28]).

The above circulation may vary in terms of the warm pool edge position $\chi(t)$, which consists of a spatial shifting movement of its entire structure in the longitudinal direction (Fig. 2, Extended Data Fig. 2, Supplementary Information Video 1). The rationale for this is simply that, from one state to another, the atmosphere and ocean approximately rebalance according to the same arguments discussed above. Such a process can be seen as a reinterpretation of the so-called Bjerknes hypothesis, that broadly speaking refers to mutual reinforcements between the Walker circulation's atmosphere and SSTs.[3] The circulation may also vary in terms of $h_W(t)$ that relates to the overall ocean heat content as detailed hereafter.

Regions averages. Let χ from Eq. 2 be the variable extent of the warm pool region with $0 \leq \chi \leq 1$. Similarly, let μ (pronounced "mu")

be the variable extent of the cold tongue region with $0 \leq \mu \leq 1$. Longitudinal (i.e. zonal) shifting results in opposite contractions and expansions of each region as encapsulated by $\chi + \mu = 1$. Here χ denotes interchangeably warm pool extent or warm pool edge position ranging from 0 to 1 in non-dimensional units: these are however distinct in dimensional units ranging respectively from 0° to 160° longitude and from 120°E to 80°W.

For a more concise representation, we introduce new indices:

$$\begin{aligned} T_W(t) &= \chi^{-1} \int_0^{\chi} T(x,t)dx \\ T_E(t) &= \mu^{-1} \int_{\chi}^{1} T(x,t)dx \\ T_M(t) &= \int_0^1 T(x,t)dx = \chi T_W + \mu T_E \end{aligned} \tag{3}$$

that represent spatial averages of SST at a given time respectively over the warm pool and cold tongue regions of variable extent and over the entire basin (Extended Data Fig. 5). Similar indices are defined for zonal wind stress (τ_W, τ_E, τ_M) and for thermocline depth (h_W, h_E, h_M). With this, the geometrical relationships from Eq. 2 can be expressed more simply as:

$$\begin{aligned} \tau_M &= \mu \tau_E \\ T_E &= T_W - s\mu \\ h_E &= h_W - a\mu \end{aligned} \tag{4}$$

which encapsulates the trade winds span over the cold tongue region as well as the sloping of SST and thermocline depth. Combining the above with the definitions of basin-wide averages (Eq. 3), we obtain nonlinear quadratic relationships:

$$\begin{aligned} T_W &= T_M + s\mu^2 \\ T_E &= T_M - s\chi\mu \\ h_W &= h_M + a\mu^2 \\ h_E &= h_M - a\chi\mu \end{aligned} \tag{5}$$

where we recall that T_W is constant. We can also deduce spatial averages over any given region of the equatorial Pacific (e.g. conventional regions Niño 4, 3.4 or 3) from Eq. 2.

The relationships in Eq. 2-5 infer the Walker circulation's geometrical response to given dynamical constraints as discussed hereafter (Fig. 3, Extended Data Fig. 6, Extended Data Tab. 1). The characteristics of the Walker circulation at a given time are set entirely by χ (or equivalently μ) and h_M, from which we deduce other variables. h_M is the spatial average of thermocline depth over the basin, also referred to as basin-wide heat content or warm water volume in the literature.[26]

Model Derivation. Consider a thermodynamical budget for the cold tongue SST and a dynamical budget for the basin-wide heat content:

$$\begin{aligned} dT_E/dt &= -\xi(T_E - T_W) + \eta h_E - Q - q^* \\ dh_M/dt &= -\sigma h_M + \gamma \tau_M + F + \zeta \end{aligned} \tag{6}$$

with relaxation parameters (ξ, σ), thermocline feedback (η), wind stress forcing (γ) and optional stochastic forcing ζ as in conventional recharge-discharge theory.[8] Modifications to this theory consist here in adding constant external sources F, Q that set equilibrium conditions (as we are working with field totals instead of anomalies), in addition to a flux $q^* = (T_E - T_W)\mu^{-1}(d\mu/dt)$ as we allow the cold tongue region to expand and contract (Leibniz integral rule). With the exception of q^*, the present starting budgets are linear as model nonlinearities will be introduced hereafter from the geometry of the problem. We also approximately omit seasonal effects for the sake of brevity. Other relationships invoked in recharge-discharge theory (e.g. atmospheric response[8]) are here disregarded: instead, we close the above budgets with the Walker circulation's geometry (Eq. 4-5).

Combining the above relationships, we obtain a minimal oscillator for the ENSO:

$$\begin{aligned} 2s(d\mu/dt) &= -\xi s\mu + a\eta(\mu - \mu^2) - \eta h_M + Q \\ dh_M/dt &= -\sigma h_M + b\mu + F + \zeta \end{aligned} \tag{7}$$

where we note $b = -\gamma\tau_E$ for brevity. The above model is nicknamed Contraction-Recharge-Expansion-Discharge Oscillator (CREDO) in reference to the original Recharge-Discharge Oscillator (RDO).[8] This is because the warm pool consecutively contracts, recharges, expands then discharges during an ENSO cycle (Extended Data Fig. 3). The model represents all major ENSO patterns as a single dynamical continuum:[5] La Niña (μ large), central Pacific El Niño (μ moderately small) and eastern Pacific El Niño (μ very small) (Fig. 1, 2).

Model Details. In order to sustain ENSO variability, we include ad-hoc stochastic forcing in the otherwise dissipated system from Eq. 7 in the

form of:

$$d\zeta/dt = -e\zeta + r\dot{W} \tag{8}$$

where ζ accounts for random fluctuations in nature (e.g. wind bursts[28]) as driven by a white noise source $\dot{W}$ with standard normal distribution[27] (Extended Data Fig. 5e).

In practice, the external sources F, Q are deduced such as to obtain a model equilibrium μ_0, h_{M0} that is comparable to observed temporal averages.[19] This reads:

$$\begin{aligned} F &= -b\mu_0 + \sigma h_{M0} \\ Q &= \xi s \mu_0 - a\eta(\mu_0 - \mu_0^2) + \eta h_{M0} \end{aligned} \tag{9}$$

where μ_0, h_{M0} are imposed. These external sources here maintain the cold tongue and control its average extent. For lower values of F and Q, it is in fact possible to obtain $\mu_0 = 0$ for which the cold tongue collapses and the equatorial Pacific is overlapped entirely by the warm pool. While these external sources may stem from a wide range of processes,[21,22] we leave their discussion for future work. The model's linear solutions around the present equilibrium consists in an oscillatory mode with period around 2.5 years and decay time around 5 months.

Extended Tab. 2 details model units and parameters. As regard numerics, we integrate the model using a simple Euler scheme in time with a timestep 0.1 mth. We constrain $0 \leq \mu \leq 1$ each timestep to deal with potential region collapses even though none occurs during the present simulation (Fig. 3a).

Potential Model Modifications. The present model is in no way a definitive theory for ENSO space-time complexity and may be extended in future work through different avenues. Building upon the existing body of work from the literature, the present framework could be combined with seasonal effects, state-dependent noise, zonal advection of SST or other SST feedbacks, and so on.[9] These modifications might help reconcile spatial shifting with other rationales for complexity, nonlinearity and mean state interactions from the literature.[6,19,20,27,29]

As a proof of concept, we have kept the model's complexity to a minimum. Suitable modifications may improve detailed yet important features of ENSO variability (Supplementary Information Video 1). For example, some central Pacific El Niños exhibit a localized SST warming just west of the warm pool edge that overshoots the warm pool saturation level 29°C imposed here. Some eastern Pacific El Niños exhibit a lingering of warm SSTs in their trail that isn't grasped by the present idealized geometry. The model representation may also be refined to account for the gradual trade winds decays towards the South American coasts, the thermocline sloping in the western Pacific, and so on.

Principal Components Reconstruction. Principal component (PC) analysis is a statistical method based on covariance that is widely used in climate sciences to deduce dominant patterns from data[30,31,34,32,33] (among other applications). Here SST in the equatorial Pacific may be reconstructed for example from its first PC or from its first and second PCs as:

$$\begin{aligned} \mathrm{R1}(x,t) &= \mathrm{PC1}(t)\mathrm{EOF1}(x) + \overline{T} \\ \mathrm{R1\&2}(x,t) &= \mathrm{R1} + \mathrm{PC2}(t)\mathrm{EOF2}(x) \end{aligned} \tag{10}$$

with associated empirical orthogonal functions (EOFs, Fig. 4a, b), where we denote here PC1 and PC2 as PC timeseries (Fig. 4c) and where $\overline{T}$ is temporal mean. The first PC alone (R1) reasonably reconstructs SST variability in the eastern and western Pacific but is severely biased in the central Pacific (Extended Data Fig. 7). In the present reconstruction R1&2, the first and second PC timeseries are approximately tied by a quadratic relationship with general form:

$$\mathrm{PC2} = a_2\mathrm{PC1}^2 + b_2\mathrm{PC1} + c_2 \tag{11}$$

that reasonably holds in observations and the proposed oscillator model (Fig. 4c, Extended Data Fig. 7). Such a relationship has received recent focus in order to diagnose ENSO nonlinearity.[32,33]

Observational Data. Observational data used in this paper is from the NCEP Global Ocean Data Assimilation System (GODAS),[44] provided by the NOAA/OAR/ESRL PSL, Boulder, Colorado, USA, from their Web site at https://www.psl.noaa.gov/data/gridded/data.godas.html. Data is monthly over 1982-2017 and includes fields of zonal wind stress ($\mathrm{N.m^{-2}}$), thermocline depth (m, measured as the 20°C isotherm) and SST (°C). All fields span the equatorial Pacific 120°E-80°W, are meridionaly averaged within 5°N-5°S and have their seasonal variations around temporal averages removed (which

we refer to as totals in the present paper with a slight abuse in terminology).

The indice χ that measures the warm pool edge position in observations (Fig. 1, 3, Extended Data Fig. 2, 3) is defined as:

$$\chi(t) = \int_0^1 \text{bool}(\text{T} > 28.5°\text{C})dx + \Delta_c \qquad (12)$$

where $T(x,t)$ is observed SST, the equatorial Pacific spans $0 \leq x \leq 1$ (120°E-80°W in dimensional units), the bool function maps 1 if the boolean condition is true and zero otherwise, and Δ_c is a constant. The estimation method is meant to delineate robustly the 29°C isotherm at which warm pool SSTs approximately saturate, but requires additional workarounds to minimize thresholding sensitivity. First, we measure the index on data without seasonal variations which simplifies the delineation. Second, a threshold value 28.5°C is chosen that, in order to allow delineation, must be slightly below the actual saturation value 29°C. In order to grasp the saturation value slightly more west, we add an empirical correction Δ_c (-10 degrees °E in dimensional units). Third, occasional cooling below 28.5°C in the far western Pacific can bias the estimation, and to remedy this we set bool= 1 west of the measured χ and recompute it once.

References

[1] Ropelewski, C.F., Halpert, M.S.: Global and regional scale precipitation patterns associated with the El Niño Southern Oscillation. Mon. Weath. Rev. **115**(8), 1606–1626 (1987)

[2] McPhaden, M.J., Zebiak, S.E., Glantz, M.H.: ENSO as an integrating concept in earth science. science **314**(5806), 1740–1745 (2006)

[3] Bjerknes, J.: Atmospheric teleconnections from the equatorial Pacific. Mon. Weath. Rev. **97**(3), 163–172 (1969)

[4] Neelin, J.D., Battisti, D.S., Hirst, A.C., Jin, F.-F., Wakata, Y., Yamagata, T., Zebiak, S.E.: ENSO theory. J. Geophys. Res. **103**(C7), 14261–14290 (1998)

[5] Capotondi, A., Wittenberg, A.T., Newman, M., Di Lorenzo, E., Yu, J.-Y., Braconnot, P., Cole, J., Dewitte, B., Giese, B., Guilyardi, E., *et al.*: Understanding ENSO diversity. Bull. Am. Meteorol. Soc. **96**(6), 921–938 (2015)

[6] An, S.-I., Tziperman, E., Okumura, Y.M., Li, T.: ENSO Irregularity and Asymmetry. In: McPhaden, M.J., Santoso, A., Cai, W. (eds.) El Niño Southern Oscillation in a Changing Climate, vol. 253, pp. 153–172. AGU, Washington DC (2020)

[7] Timmermann, A., An, S.-I., Kug, J.-S., Jin, F.-F., Cai, W., Capotondi, A., Cobb, K.M., Lengaigne, M., McPhaden, M.J., Stuecker, M.F., *et al.*: El Niño–Southern Oscillation complexity. Nature **559**(7715), 535–545 (2018)

[8] Jin, F.-F.: An equatorial ocean recharge paradigm for ENSO. Part I: Conceptual model. J. Atmos. Sci. **54**(7), 811–829 (1997)

[9] Jin, F.-F., Chen, H.-C., Zhao, S., Hayashi, M., Karamperidou, C., Stuecker, M.F., Xie, R., Geng, L.: Simple ENSO Models. In: McPhaden, M.J., Santoso, A., Cai, W. (eds.) El Niño Southern Oscillation in a Changing Climate, vol. 253, pp. 119–151. AGU, Washington DC (2020)

[10] Kug, J.-S., Jin, F.-F., An, S.-I.: Two types of El Niño events: cold tongue El Niño and warm pool El Niño. J. Clim. **22**(6), 1499–1515 (2009)

[11] Kao, H.-Y., Yu, J.-Y.: Contrasting eastern-Pacific and central-Pacific types of ENSO. J. Clim. **22**(3), 615–632 (2009)

[12] McPhaden, M.J.: Genesis and evolution of the 1997-98 El Niño. Science **283**(5404), 950–954 (1999)

[13] Barnston, A.G., Tippett, M.K., L'Heureux, M.L., Li, S., DeWitt, D.G.: Skill of real-time seasonal ENSO model predictions during 2002–11: Is our capability increasing? Bull. Am. Meteorol. Soc. **93**(5), 631–651 (2012)

[14] Bellenger, H., Guilyardi, E., Leloup, J.,

Lengaigne, M., Vialard, J.: ENSO representation in climate models: From CMIP3 to CMIP5. Clim. Dyn. **42**(7), 1999–2018 (2014)

[15] Ham, Y.-G., Kug, J.-S.: How well do current climate models simulate two types of El Niño? Clim. Dyn. **39**(1), 383–398 (2012)

[16] Guilyardi, E., Capotondi, A., Lengaigne, M., Thual, S., Wittenberg, A.T.: ENSO Modeling: History, Progress and Challenges. In: McPhaden, M.J., Santoso, A., Cai, W. (eds.) El Niño Southern Oscillation in a Changing Climate, vol. 253, pp. 199–226. AGU, Washington DC (2020)

[17] Takahashi, K., Dewitte, B.: Strong and moderate nonlinear El Niño regimes. Clim. Dyn. **46**(5), 1627–1645 (2016)

[18] Xie, R., Jin, F.-F.: Two leading ENSO modes and El Niño types in the Zebiak–Cane model. J. Clim. **31**(5), 1943–1962 (2018)

[19] Timmermann, A., Jin, F.-F., Abshagen, J.: A nonlinear theory for El Niño bursting. Journal of the atmospheric sciences **60**(1), 152–165 (2003)

[20] An, S.-I., Jin, F.-F.: Nonlinearity and asymmetry of ENSO. J. Clim. **17**(12), 2399–2412 (2004)

[21] Dijkstra, H.A., Neelin, J.D.: Ocean-atmosphere interaction and the tropical climatology. Part II: Why the Pacific cold tongue is in the east. J. Clim. **8**(5), 1343–1359 (1995)

[22] Xie, S.-P.: Ocean–atmosphere interaction in the making of the Walker circulation and equatorial cold tongue. J. Clim. **11**(2), 189–201 (1998)

[23] Schopf, P.S., Burgman, R.J.: A simple mechanism for ENSO residuals and asymmetry. J. Clim. **19**(13), 3167–3179 (2006)

[24] Picaut, J., Masia, F., du Penhoat, Y.: An advective-reflective conceptual model for the oscillatory nature of the ENSO. Science **277**(5326), 663–666 (1997)

[25] Clarke, A.J., Wang, J., Van Gorder, S.: A simple warm-pool displacement ENSO model. J. Phys. Oceanogr. **30**(7), 1679–1691 (2000)

[26] Meinen, C.S., McPhaden, M.J.: Observations of warm water volume changes in the equatorial Pacific and their relationship to El Niño and La Niña. J. Clim. **13**(20), 3551–3559 (2000)

[27] Jin, F.-F., Lin, L., Timmermann, A., Zhao, J.: Ensemble-mean dynamics of the ENSO recharge oscillator under state-dependent stochastic forcing. Geophys. Res. Lett. **34**(L03807) (2007)

[28] Vecchi, G.A., Harrison, D.: Tropical pacific sea surface temperature anomalies, El Niño, and equatorial westerly wind events. J. Clim. **13**(11), 1814–1830 (2000)

[29] Chen, N., Fang, X., Yu, J.-Y.: A multiscale model for el Niño complexity. npj Clim. Atmos. Sci. **5**(16) (2022)

[30] Takahashi, K., Montecinos, A., Goubanova, K., Dewitte, B.: ENSO regimes: Reinterpreting the canonical and Modoki El Niño. Geophys. Res. Lett. **38**(L10704) (2011)

[31] Dommenget, D., Bayr, T., Frauen, C.: Analysis of the non-linearity in the pattern and time evolution of El Niño Southern Oscillation. Clim. Dyn. **40**(11), 2825–2847 (2013)

[32] Karamperidou, C., Jin, F.-F., Conroy, J.L.: The importance of ENSO nonlinearities in tropical Pacific response to external forcing. Clim. Dyn. **49**(7), 2695–2704 (2017)

[33] Cai, W., Wang, G., Dewitte, B., Wu, L., Santoso, A., Takahashi, K., Yang, Y., Carréric, A., McPhaden, M.J.: Increased variability of eastern Pacific el Niño under greenhouse warming. Nature **564**(7735), 201–206 (2018)

[34] Stuecker, M.F., Timmermann, A., Jin, F.-F., McGregor, S., Ren, H.-L.: A combination mode of the annual cycle and the El Niño Southern Oscillation. Nature Geoscience **6**(7), 540–544 (2013)

[35] Martinez-Villalobos, C., Vimont, D.J.: An analytical framework for understanding tropical meridional modes. J. Clim. **30**(9), 3303–3323 (2017)

[36] Fedorov, A.V., Hu, S., Wittenberg, A.T., Levine, A.F.Z., Deser, C.: ENSO Low-Frequency Modulation and Mean State Interactions. In: McPhaden, M.J., Santoso, A., Cai, W. (eds.) El Niño Southern Oscillation in a Changing Climate, vol. 253, pp. 173–198. AGU, Washington DC (2020)

[37] Cai, W., Wu, L., Lengaigne, M., Li, T., McGregor, S., Kug, J.-S., Yu, J.-Y., Stuecker, M.F., Santoso, A., Li, X., *et al.*: Pantropical climate interactions. Science **363**, 4236 (2019)

[38] Yun, K.-S., Timmermann, A., Stuecker, M.F.: Synchronized spatial shifts of Hadley and Walker circulations. Earth Syst. Dynam. **12**(1), 121–132 (2021)

[39] Klein, S.A., Soden, B.J., Lau, N.-C.: Remote sea surface temperature variations during ENSO: Evidence for a tropical atmospheric bridge. J. Clim. **12**(4), 917–932 (1999)

[40] Jin, F.-F., Kim, S.T., Bejarano, L.: A coupled-stability index for ENSO. Geophys. Res. Lett. **33**(L23708) (2006)

[41] Vijayeta, A., Dommenget, D.: An evaluation of ENSO dynamics in CMIP simulations in the framework of the recharge oscillator model. Clim. Dyn. **51**(5), 1753–1771 (2018)

[42] Fedorov, A.V., Philander, S.G.: A stability analysis of tropical ocean–atmosphere interactions: Bridging measurements and theory for El Niño. J. Clim. **14**(14), 3086–3101 (2001)

[43] Wittenberg, A.T.: Are historical records sufficient to constrain ENSO simulations? Geophys. Res. Lett. **36**(L12702) (2009)

[44] Behringer, D., Xue, Y.: Evaluation of the global ocean data assimilation system at NCEP: The Pacific Ocean. In: Proc. Eighth Symp. on Integrated Observing and Assimilation Systems for Atmosphere, Oceans, and Land Surface (AMS 84th Annual Meeting) (2004)

Extended Data Tab. 1 Indices statistics.

Indice	Mean		Std		Skewness	
	Model	Obs	Model	Obs	Model	Obs
χ (1000 km)	6.61	6.56	2.43	1.96	0.92	1.44
τ_W (10^{-3} N.m^{-2})	0	-10	0	7.8	0	0.45
τ_M	-22	-26	4.7	5.8	0.92	0.09
τ_E	-35	-35	0	0.6	0	0.27
h_W (m)	165	165	12.8	12.5	-1.1	-0.63
h_M	124	125	8.4	6.3	-0.25	-0.85
h_E	102	104	7.0	7.7	-0.33	-0.22
T_W (°C)	29.0	29.4	0	0.25	0	-0.24
T_M	27.1	27.5	0.71	0.53	0.11	0.34
T_E	26.2	26.4	0.61	0.55	0.92	0.98
Niño 4 SST °C	28.3	28.5	0.63	0.67	-0.89	-0.45
Niño 3.4 SST	27.4	27.5	0.88	0.81	-0.18	0.06
Niño 3 SST	25.7	25.8	1.14	0.93	0.57	0.97

Extended Data Tab. 2 Model units and parameters.

Parameter	Value	Scaling	Definition
$[x]$	1	18000 km	unit zonal position
$[t]$	1	1 month	unit time
$[h]$	1	20 m	unit thermocline depth
$[T]$	1	1 °C	unit SST
$[\tau_x]$	1	0.01 N.m^{-2}	unit zonal wind stress
L	1	18 000 km	equatorial Pacific length
T_W	29	29°C	saturation level SST
s	4.5	0.25 °C.(1000 km)$^{-1}$	sloping rate SST (halved)
a	5	5.56 m.(1000 km)$^{-1}$	sloping rate thermocline (halved)
ξ	1/6	(6 mth)$^{-1}$	relaxation SST
σ	1/14	(14 mth)$^{-1}$	relaxation thermocline
b	0.7	7.8 10^{-7} mth^{-1}	trade winds constant
η	0.8	0.04 °C.m^{-1}.mth^{-1}	thermocline feedback
Q	4.56	4.56 °C.mth^{-1}	external cooling
F	-1.6 10^{-3}	-0.37 m.yr^{-1}	external forcing
μ_0	0.36	6480km	equilibrium value of μ
h_{M0}	6.25	125m	equilibrium value of h_M
e	1/3	(3 mth)$^{-1}$	stochastic forcing dissipation
r	0.1	2 m.mth^{-2}	stochastic forcing generation
Δ_c	-0.0625	-10 deg °E	correction for χ (in observations)

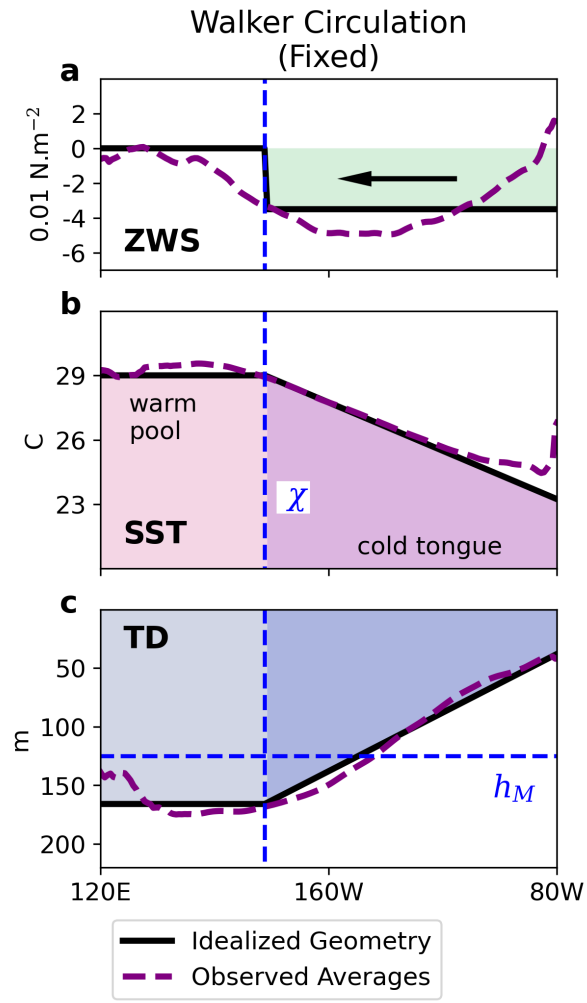

Extended Data Fig. 1 Walker circulation structure. Zonal profiles of zonal wind stresses (ZWS, **a**), sea surface temperatures (SST, **b**) and thermocline depth (TD, **c**) in a longitudinal strip spanning the equatorial Pacific (black lines and fillings). The circulation can only vary in terms of its warm pool edge position χ, except for thermocline depth that can additionally vary in terms of its basin-wide average h_M (blue dashed lines). As a proof of concept we adjust these variables in the figure in order to match observed temporal averages of ZWS, SST and TD (purple dashed lines).

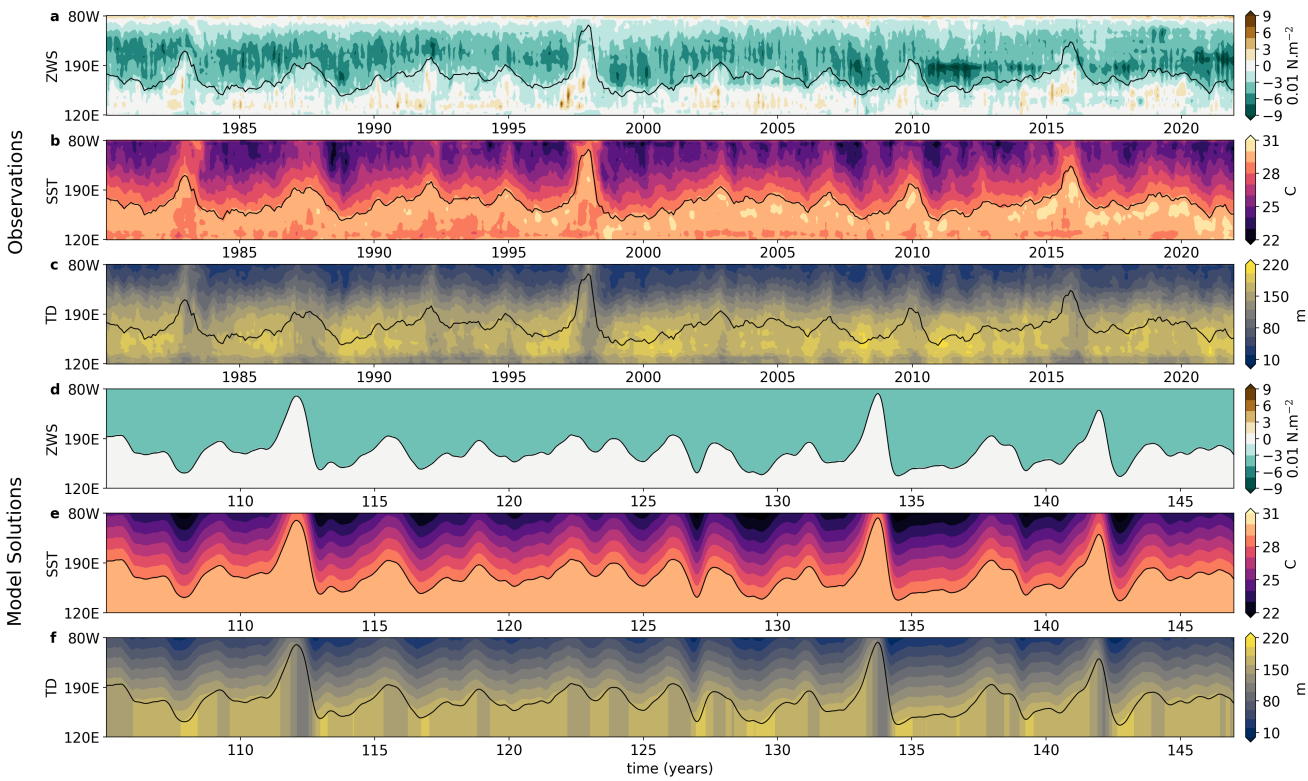

Extended Data Fig. 2 Time-longitude hovmollers for totals. **a,b,c**, Time-longitude hovmollers of zonal wind stress (ZWS), sea surface temperature (SST) and thermocline depth (TD) in the equatorial Pacific, as computed from observations (averaged 5°N-5°S with seasonal variations removed). **d,e,f**, Analysis repeated for the outputs of the oscillator model (displayed over a hand-picked period). Solid lines in each panel indicate the longitudinal position of the warm pool edge (i.e. 29°C SST isotherm, see methods). The spatial shifting of the Walker circulation consists of a general and coherent longitudinal movement of the atmospheric and oceanic structures that follows the warm pool edge, as found in observations and as reproduced qualitatively by the oscillator model. The movement is less apparent on thermocline depth that also varies significantly in terms of its basin-wide average.

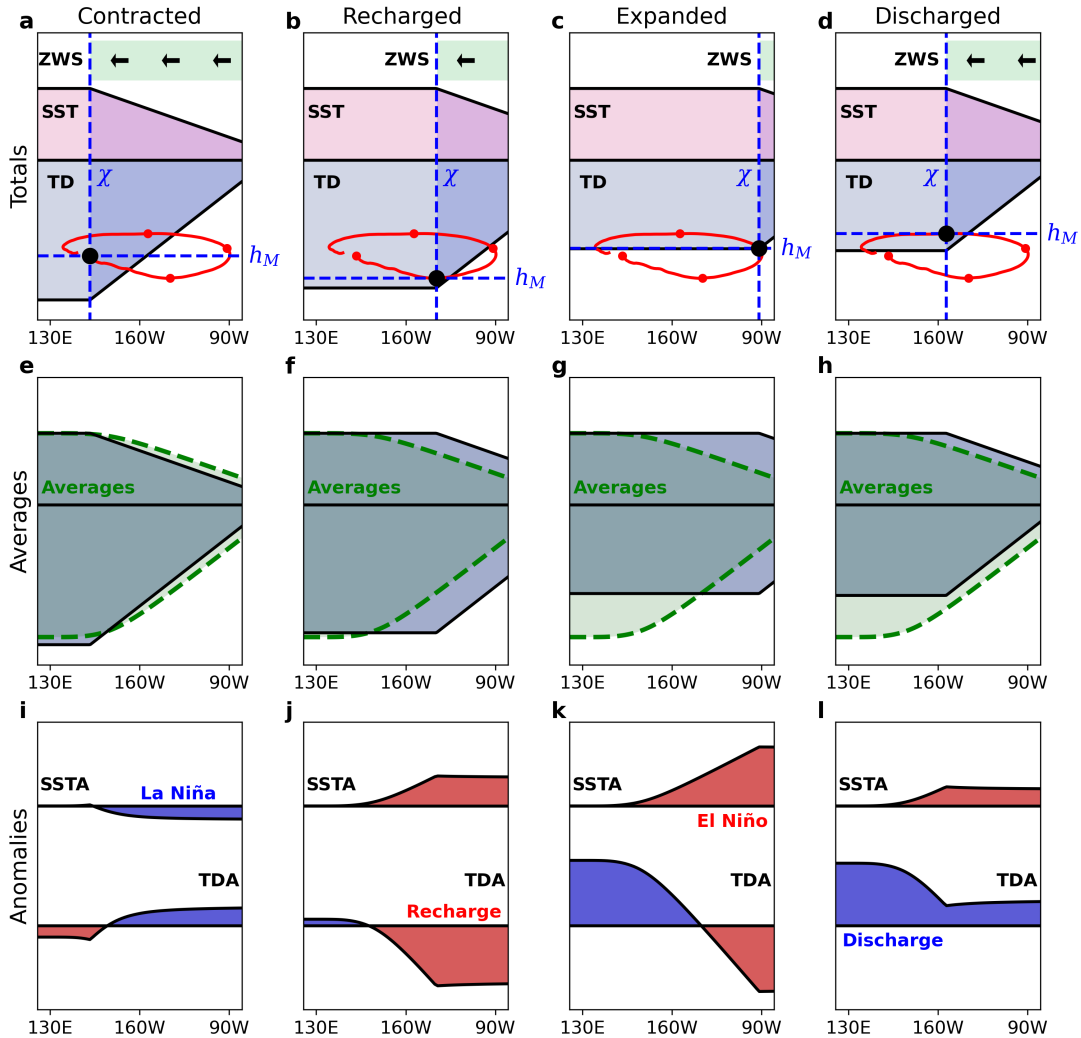

Extended Data Fig. 3 ENSO cycle in the oscillator model. **a-d**, Sketch of the Walker circulation at the four consecutive stages of one ENSO cycle: contracted (La Niña), recharged, expanded (El Niño) and discharged. This is shown for zonal wind stress (ZWS), sea surface temperatures (SST) and thermocline depth (TD) represented as in Extended Data Fig. 1. The circulation is entirely determined by the warm pool extent χ and basin-wide heat content h_M, indicated at each stage of the cycle (blue dashed lines) and for the entire cycle (red lines, years 132 to 135 in Fig. 1)). **e-h**, Mean state of SST and TD (i.e. temporal averages computed over the entire simulation, green dashed lines) with total fields from a-d repeated (gray fillings). **i-l**, Sea surface temperature anomalies (SSTA) and thermocline depth anomalies (TDA) at each stage as computed with respect to the mean state. The oscillator model generates ENSO cycles that follow a conventional recharge-discharge evolution of heat content but where SSTA and TDA patterns stem from the Walker circulation's movements.

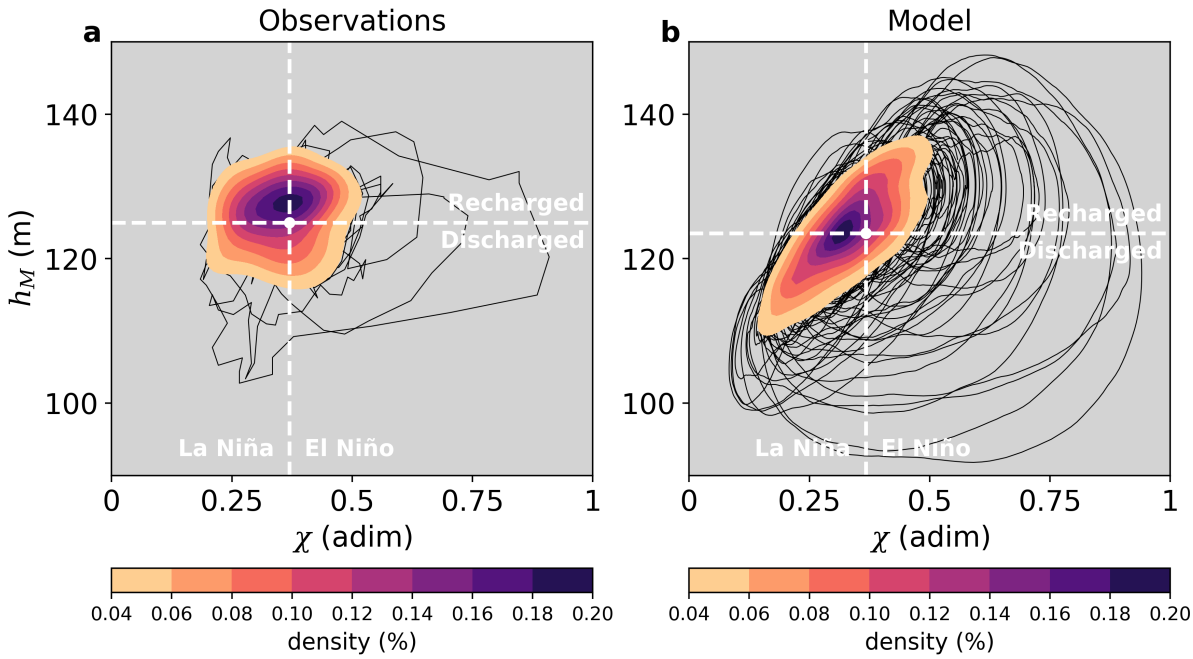

Extended Data Fig. 4 Phase space comparison. Kernel density estimates (contours) and individual realizations (black lines) in phase space of warm pool extent χ and basin-wide heat content h_M, in either observations (**a**) or model solutions (**b**). For clarity, density estimates are shown only above 0.04% where they hide individual realizations that are too dense to visualize. Phase space is divided into El Niño or La Niña states as well as recharged or discharged states as defined here with respect to average conditions (white dashed lines). El Niño events may reach larger amplitudes than La Niña events but are more short-lived.

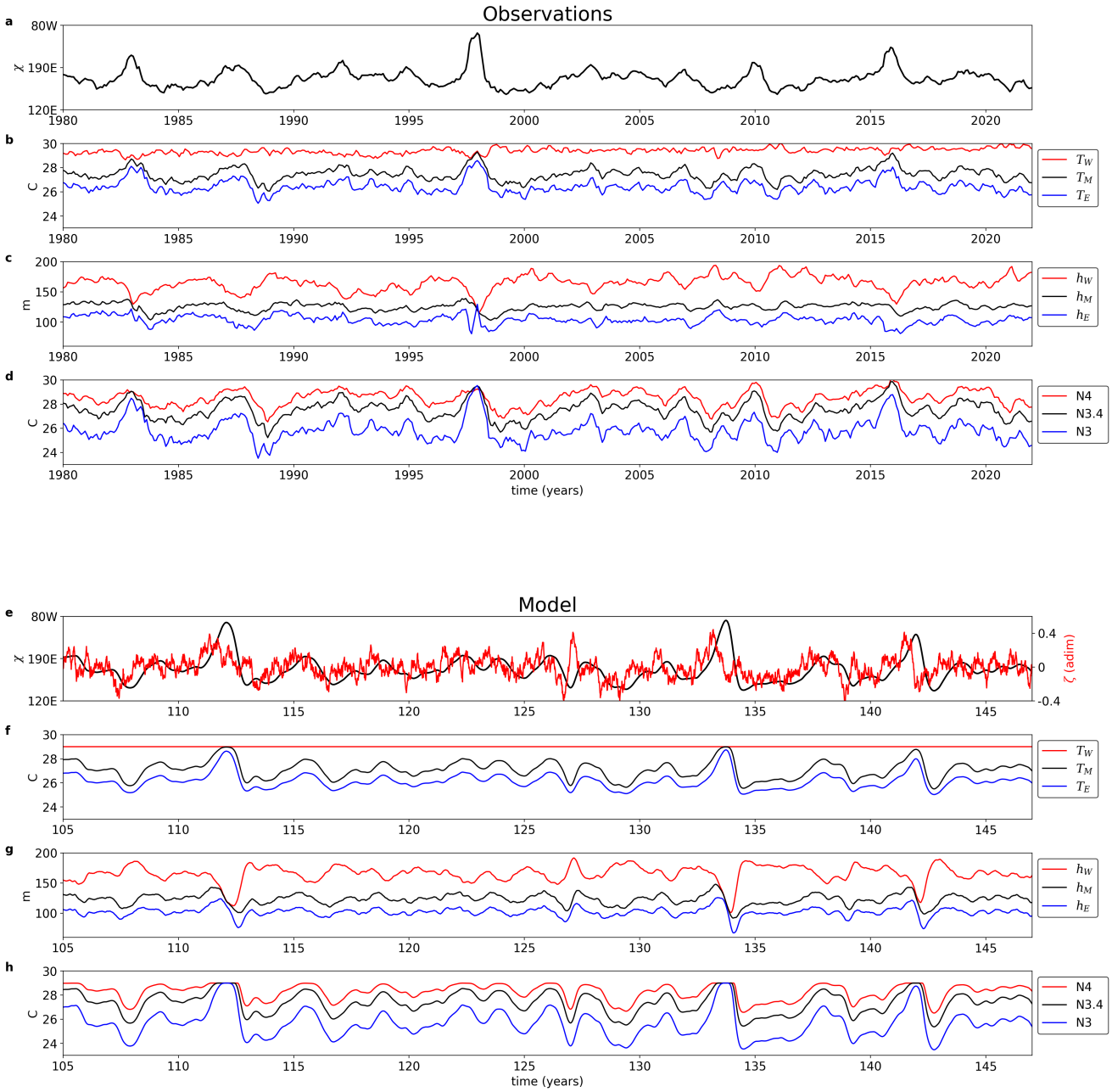

Extended Data Fig. 5 Indices timeseries. Timeseries from observations of warm pool edge position (**a**), SST spatial averages (**b**), thermocline depth spatial averages (**c**), and indices Niño 4 (N4), Niño 3.4 (N34) and Niño 3 (N3) SST (**d**). **e-h**, Analysis repeated for outputs of the oscillator model displayed over a hand-picked period. We also show the ad-hoc stochastic forcing ζ in the oscillator model (e, red line). The indices T_W, T_E, T_M (h_W, h_E, h_M) averages SST (thermocline depth) conditions respectively over the warm pool, cold tongue and entire basin (120°E-80°W). The conventional indices Niño 4, 3.4 and 3 SST average conditions over the central (160°E-150°W), central-eastern (170°W-120°W) and eastern (150°W-90°W) Pacific. All averages are within the equatorial band (5°N-5°S).

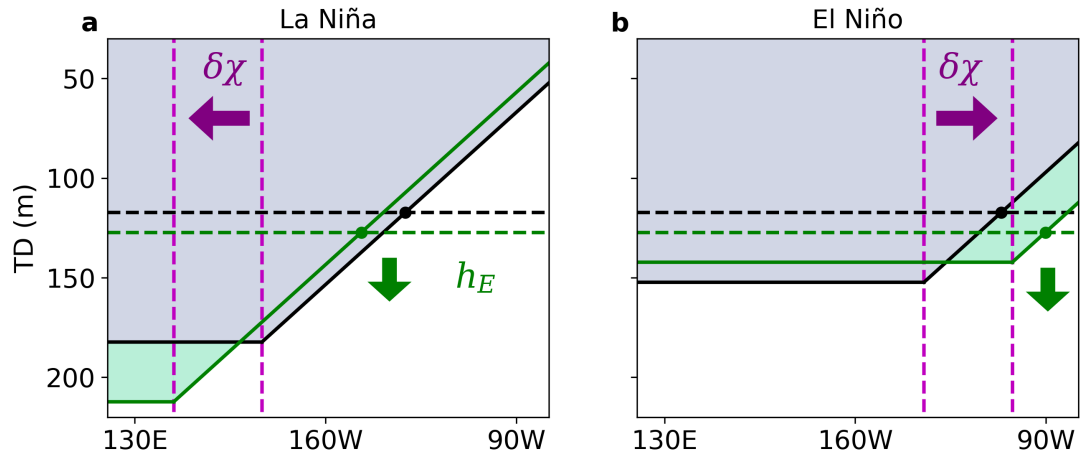

Extended Data Fig. 6 Thermocline nonlinearity. Starting from either a La Niña state (**a**) or El Niño state (**b**), we apply a zonal shifting perturbation $\delta\chi$ (at constant basin-wide heat content h_M) that further develops the corresponding event (purple dashed lines). We then compare the original thermocline depth profile (gray filling) versus the modified one (green filling). The thermocline depth averaged over the cold tongue h_E increases in both cases (dots and dashed lines). This generates asymmetry as it mitigates La Niña development but amplifies El Niño development. The relationship is encapsulated by $h_E = h_M - a(\chi - \chi^2)$ in the oscillator model (see methods).

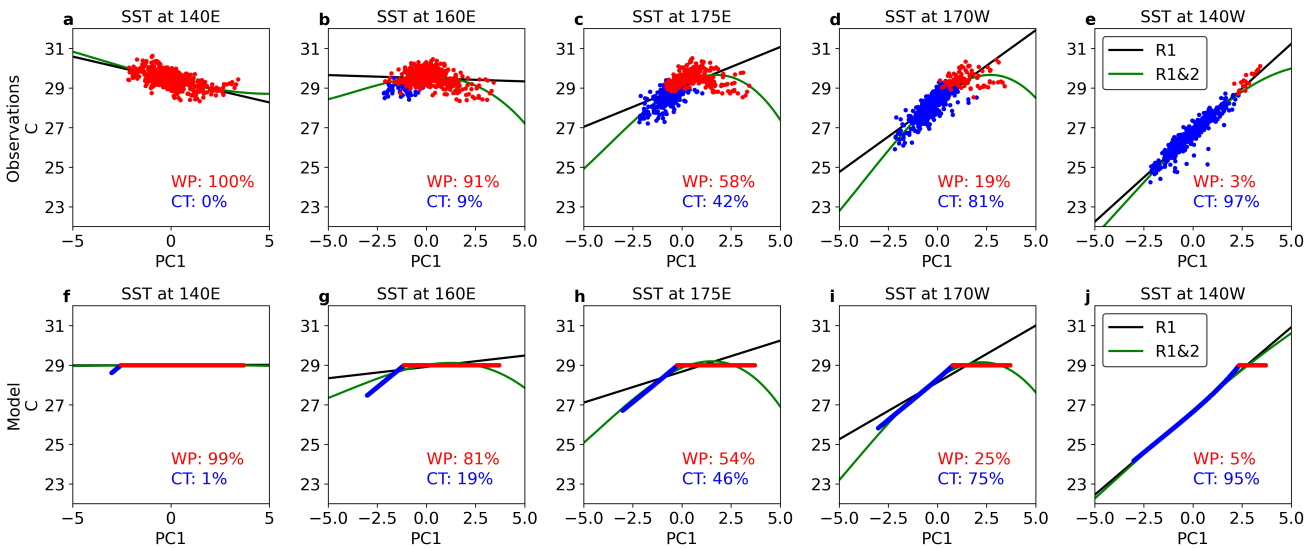

Extended Data Fig. 7 Principal components reconstruction. **a-e**, Scatter plots between sea surface temperatures (SST) and first principal component timeserie (PC1) at different longitudes of the equatorial Pacific, as computed from observations. **f-j**, Analysis repeated for outputs of the oscillator model. Individual realizations are discriminated in terms of their belonging to the warm pool region (WP, red) or cold tongue region (CT, blue), with total occurrences indicated in %. We show SST reconstructed from first principal component (R1, black lines), as well as SST reconstructed from first and second principal components (R1&2, green lines) for which PC2 approximately depends on PC1 through a quadratic relationship (Fig. 4 and methods). First principal component alone (R1) captures well "pure" WP or CT characteristics in the western and eastern Pacific, but fails to capture nonlinearly mixed WP-CT characteristics in the central Pacific. These mixed WP-CT characteristics have approximately a quadratic shape that is captured instead by a joint reconstruction from first and second principal components (R1&2).

Supplementary Material Video 1 Evolution of the Idealized Walker Circulation. **a,e,f**, Idealized Walker circulation (black lines) compared to observations (purple dashed lines) in terms of zonal wind stresses (ZWS), SST and thermocline depth (TD), where each animated frame corresponds to a given month of the record. The idealized Walker circulation is entirely determined by warm pool edge position and zonal mean thermocline depth (blue dashed lines), which values here match the ones from observations. **b,c,d**, longitude-time hovmollers of ZWS, SST and TD, with indication of warm pool edge position (blue dashed lines) and time of current frame (purple dashed lines). The idealized circulation's geometry compares reasonably to observations including for individual ENSO events.

File SI_Video_1.mp4 or link
https://drive.google.com/file/d/1BJmSKkDtvi60t9_u40Vck7-8d7i2KL1X/view?usp=sharing